Hybrid Indoor Positioning System for First Responders

Francesca De Cillis, *Student Member, IEEE,* Luca Faramondi, *Student Member, IEEE,* Federica Inderst, *Student Member, IEEE,* Stefano Marsella, Marcello Marzoli, Federica Pascucci, *Member, IEEE,* and Roberto Setola *Senior Member, IEEE*

***Abstract*—In the last decade, many efforts have been devoted to indoor localization and positioning. In this paper, a hybrid indoor localization system has been developed within the European project REFIRE for emergency situations. The REFIRE solution estimates the user's pose according to a prediction-correction scheme. The user is equipped with a waist-mounted inertial measurement unit and a RFID reader. In the correction phase the estimation is updated by means of geo-referenced information fetched from passive RFID tags pre-deployed into the environment. Accurate position correction is obtained through a deep analysis of the RFID system radiation patterns. To this end, extensive experimental trials have been performed to assess the RFID system performance, both in static and dynamic operating conditions. Experimental validation in realistic environments shows the effectiveness of the proposed indoor localization system, even during long-last missions and/or using a limited number of tags.**

***Index Terms*—Emergency services, Inertial navigation, Bayes procedures, Tracking.**

I. Introduction

INdoor localization and positioning system enables the use of location services in indoor environments, where people spend most of their time (e.g., working, shopping, eating, etc.) in different locations (e.g., malls, offices, campus, etc.) and where the traditional GPS system cannot be used. Localization and tracking support is useful in many contexts [4] (e.g., key building management, retail industry, personal services, etc.), but it becomes crucial in emergency response scenarios: being aware of team location is essential for an effective rescue mission management.

In large and complex indoor emergency scenario, first responders need to know their exact locations, possible escaping routes, and potential risks (e.g. machineries, hazardous materials, etc.) in the surrounding area. Properly localized and well informed about risks, rescuers can be better coordinated, commanded, and guided, thus reducing the possibility of disorientation and/or failures in localizing victims.

In an emergency scenario, requirements are severe [23], [24]: for example, indoor localization for first responders cannot relies only on an external infrastructure, since it could result unavailable during emergencies. At the same time, high tech and heavy equipment cannot be adopted due to the harsh operating conditions. A possible solution is the use of small and lightweight wearable devices that should be designed as robust as possible to withstand rough handling and very high temperatures. Finally, a reliable and accurate position information should be provided continuously by the localization system. The lack of an efficient indoor localization methodology for rescuers pushes the research towards alternative localization systems specifically designed for emergencies.

In this paper, the REFIRE Hybrid Indoor Positioning System (HIPS) is presented: it integrates inertial navigation system with a smart environment based on RFID (Radio Frequency IDentification) technology for assessing personal indoor localization and tracking. Using the Pedestrian Dead Reckoning (PDR) approach [10], the information collected from Inertial Measurement Unit (IMU) is processed to provide an estimate about the operator's relative pose (i.e., position and heading). The HIPS flips over the common RFID-based approach commonly used for object localization and tracking: the environment is kitted out with pre-deployed RFID passive tags provided with information about their absolute geographical position. The HIPS is able to reduce the drift error which affects the inertial system by using a limited set of RFID tags: location data fetched from tags are used to reset the user position estimate. To facilitate the sensors deployment and to fit the coverage, the REFIRE framework considers to embed passive tags into emergency lights.

With respect to the state of the art, several contributions are presented in this paper. The proposed PDR algorithm processes data from a waist-mounted IMU, rather than using a foot–mounted one, as presented by most of the approaches in the literature. Moreover, RFID are used to provide context information: to this end, a large assessment on the RFID performance is reported. Outcomes from the experimental trials allow the definition of a suitable correction strategy based on context information merged in a Bayesian framework, that represents the main novelty of the paper. In HIPS, *a–priori* knowledge is not considered: the tags deployed in the environment provide all the information to improve tracking accuracy. Finally, the proposed infrastructure (i.e., RFID tags

Manuscript received February 20, 2017; revised May 29, 2017. This work was supported by the European Commission, Directorate, General Home Affairs, Grant Home/2010/CIPS/AG/033 REFIRE - REference implementation of interoperable indoor location & communication systems for FIrst REsponders.

F. De Cillis, L. Faramondi and R. Setola are with the Complex Systems and Security Lab, Università Campus Bio-Medico di Roma, Rome, Italy e-mail: f.decillis@unicampus.it, l.faramondi@unicampus.it, r.setola@unicampus.it

L. Faramondi, F. Inderst, and F. Pascucci are with the Dipartimento di Ingegneria, Università degli Studi Roma Tre, Rome, Italy e-mail: luca.faramondi@uniroma3.it, federica.inderst@uniroma3.it, federica.pascucci@uniroma3.it

S. Marsella, M. Marzoli are with the Dipartimento dei Vigili del Fuoco, S.P. e D.C., Ministero dell'Interno, Rome, Italy e-mail: stefano.marsella@vigilfuoco.it, marcello.marzoli@vigilfuoco.it

and reader) has been largely tested to get insights on the reliability and the accuracy of the localization system.

The paper is organized as follows. In Section II a review on IPL for rescuers is reported. In Section III the HIPS architecture is described and the navigation algorithm (i.e., attitude and tracking systems) detailed. The assessment of RFID system is presented in Section III-B. Section V reports experimental results about HIPS, and, finally, in Section VI concluding remarks and future developments are drawn.

II. Related Works

In recent years, several solutions have been proposed by the academy and the industry to solve the ILP problem. Therefore, a large amount of different methodologies has been presented. In the following, a critical investigation of most promising ILP methodologies is introduced. Most of the methodologies presented in the literature can be roughly classified into three main categories. Mass-market applications for indoor positioning require the use of standard devices without supplementary physical components, since the consumer market cannot easily accept major modifications to smartphones to include positioning functions [7]. To this end, proposed approaches rely on external infrastructure (i.e., *infrastructure–based*) predeployed in the environment (e.g., Wi-Fi signal) exploiting trilateration or fingerprinting techniques to determine the position of a user. However, in an emergency scenario, the requirements are quite severe and first responders cannot rely on an external infrastructure, that could result unavailable during emergencies. Most of the algorithms refer to proprioceptive sensors able to compute the displacement of the pedestrian by measuring human activity (i.e., *infrastructure–less*). Finally, the most effective approaches are based on the *hybridization* of proprioceptive and exteroceptive sensors.

Infrastructure-based systems require dedicated local infrastructures and/or customized mobile units, and typically use video [34], laser scanner [30] or wireless technologies (i.e., Wi-Fi [37], Zigbee [13], RFID [18], [6], ultrasound [29], Ultra-WideBand (UWB) [38], Bluetooth [39], [5], Pseudolite [4], infra-red [11]), for localization and tracking. According to [22], [31], wireless-based systems are the most widespread ones. In this category, a primary role is played by the RFID technology, because of its limited cost for both installation and maintenance. Methods exploiting RFID for pedestrian ILP are commonly divided into tag-based, reader-based, and transceiver-free. In tag-based approaches, the user is equipped with a tag, while readers are deployed in the environment. In [25], two different tags (i.e., reference tags and tracking tags attached to the users) are exploited and the correlation among RF signals is used to localize the moving tags with an accuracy of about 2 m in a small environment ($\sim 24\ m^2$). In [15], a RFID indoor personnel location tracking system for foreign visitors is proposed. Visitors are equipped with wearable RFID tag identified by readers deployed in the environment. In [3], a localization system exploiting Wi-Fi technologies is designed: the RFID tags are used to identify entities inside a building. In [9], a textile RFID tag is proposed to implement solution for human positioning and tracking applications: RFID readers and Wi-Fi receivers are jointly used to improve the localization accuracy. In reader-based localization systems, the roles of tag and reader are reversed: tags are placed at fixed and known locations; a portable reader is carried by the mobile user or by the object being tracked [20]. In [26], the human body effect on indoor localization is evaluated. The location of a RFID reader on a human body is estimated on the basis of the known locations of the RFID tags attached to the ceiling with 60 cm separation between one and another. In [8], the PERCEPT system is introduced to support blind and visually-impaired people. It is based on a RFID reader embedded in the tip of the white cane and RFID tags deployed in the environment in known positions. The user is localized by reading the information in the RFID tags. In [14], a RFID and ZigBee integrated system for indoor localization is proposed. K-Nearest Neighbor algorithm is adapted to predict the location of a user in an indoor environment. In [1], a tour guide system is proposed: it provides personalized audio-visual information based on the location of the visitor. Localization is performed deploying iBeacons and RFID tags to identify objects in the environment. Finally, in transceiver-free technologies target objects can be localized without carrying any device. This methodology is used in [19], where RFID readers and tags are deployed in the environment and the distortion of the radio frequency signal identifies the position of the user. In [17], passive tags are spatially distributed in such a manner that it is possible to infer the spatial correlation of received signal strength and to use such relationship for localization process. In [27], the human-object interaction events are considered to localize users in a furnished home by using RFID-based localization system. Adopting the infrastructure-based approaches, the major concern is related to the signal quality, due to shadowing, interferences, and lack of line of sight. A further issue is related to the large number of anchor nodes to be deployed in the environment to achieve a reasonable level of accuracy when using trilateration of fingerprinting. In emergency scenario, the only use of external infrastructure is not acceptable; however, in [16], [32] it is foreseen the deployment on-the-fly of anchor nodes within the emergency area in ad-hoc positions by the rescuer team throughout the mission.

Infrastructure-less systems use stand-alone and wearable sensors to estimate the relative location (i.e., the change in position since the last update): these systems are useful to continuously track the user. Typical infrastructure-less solutions consist in PDR based on IMU: the most common approach is based on step-and-heading. The fundamental cycle of step-and-heading is based on three phases: the identification of subsets of the data corresponding to individual strides; the estimation of the step length; the estimation of the step heading (i.e., the motion direction). Although widely investigated, PDR approaches suffer from several inaccuracy sources: the first one is related to the model used to map inertial measurements into position; the second one concerns the noise and the bias that affect the inertial measurements. Moreover, the initial pose of the user need to be known to provide absolute localization.

To overcome the drawbacks of both infrastructure-based and infrastructure-less approaches, *hybrid* systems seem to

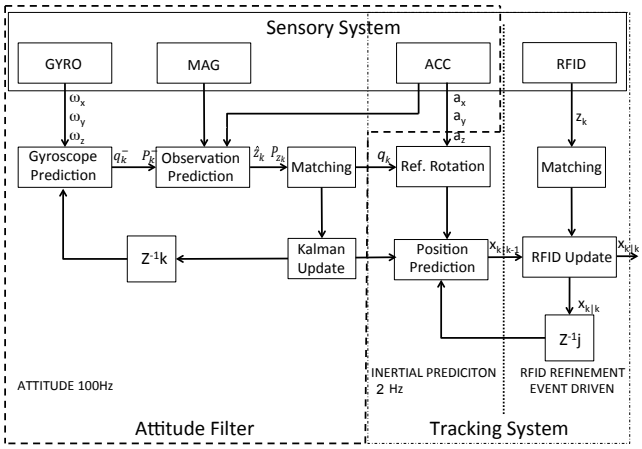

Fig. 1. The Hybrid Indoor Positioning System architecture.

be promising. They exploit advantages arising from both methods, by combining information from exteroceptive and proprioceptive sensors. In [28], the multi-sensor pedestrian navigation system IndoorGuide is presented. It is a modular solution that combines two IMUs and barometers placed on the torso and on the foot of the user, with a stereo-camera attached on the torso sensors. An Indoor Positioning System based on a combination of data collected by foot-mounted IMU, magnetometer, and UWB signals is described in [21]. An anchor-free approach is adopted and the UWB is used for ranging and communications. Experimental results show an average positioning error of about $24\ cm$.

As stated before, in this contribution, a hybrid approach for rescue localization based on PDR is proposed. However, it exploits a waist-mounted IMU rather than a foot-mounted one to enhance the wearability and the robustness of the device. The PDR drift is bounded by a reader-based RFID system: the correction is performed using context information to reduce the number of the tags pre-deployed in the environment to achieve a suitable accuracy. All localization information is stored in tag memory. In the literature, most of the approaches exploit signal strength to retrieve ranging measurements also considering other radio frequency signals (e.g., Wi-Fi, Bluetooth, ZigBee). On the contrary, this work proposes a different approach: RFID tags provide context information and they are merged with inertial estimate.

III. Hybrid Indoor Positioning System

The rescue localization problem can be addressed as finding the position (x, y) and the heading (ϕ) of the mobile agent (i.e., the rescuer) with respect to a fixed Cartesian reference frame, namely *Navigation frame*.

As stated by Italian National Fire Corps, the localization system should:

- locate the mobile agents using lightweight wearable sensors;
- exploit, when available, a network pre-deployed in the environment;
- guarantee room-level accuracy;
- provide and continuously update the position estimate;
- adopt low cost devices and computational efficient solutions.

According to rescuers' suggestions, a complete disaster scenario is not considered, since the actions required would be different from the simple exploration by walking and resting. Therefore, in this contribution, the problem of supporting rescue activities when the human perception fails, due to the presence of thick smoke and fire, is addressed. It represents a large part of the emergency situations faced by rescuers.

The proposed HIPS envisages the use of Mobile Terminals (MTs) carried by the rescuer and low-cost highly standardized Pre-Installed Location Devices (PILDs). The HIPS architecture generalizes the approach proposed by authors in [6]. In the REFIRE implementation, the MT consists of a sensory system (i.e., an inertial platform integrating a tri-axial accelerometer, a tri-axial gyroscope, a tri-axial magnetometer, and a RFID reader) connected to a processing unit, while PILDs correspond to RFID passive tags. To fulfill the requirements provided by rescuers, the IMU is a lightweight wearable device. It is a waist–mounted one, easy to integrate into the firefighter gear without using a wireless body area network for data transfer. With respect to the foot-mounted IMU [10], the proposed waist-mounted IMU less susceptible to damages. Moreover, it downgrades the PDR performance during the mission, since the zero-velocity update, which determine the step event and reset the bias, cannot be used.

The RFID reader, together with the processing unit, is placed on the left shoulder of the rescuer. As mentioned before, RFID tags are embedded within existing safety devices (e.g., emergency lights, signs, etc.). To reduce the needs for any external sources, the HIPS exploits the capability of RFID tags to store critical up-to-date building information for local retrieval. The HIPS strategy exploits IMU data with the PDR algorithm to continuously estimate the rescuer position and to correct when the rescuer approaches to a PILD. According to the REFIRE standard, no *a–priori* knowledge (i.e., maps of the RFID beacons) is provided to the rescuer, since the localization message is recorded in the user memory of the RFID tag. The message is composed of seven fields:

- *REFIRE id*;
- *Geographical coordinates* provided adopting the WGS-84 standard for cartography, geodesy, and navigation;
- *Device classification* identifies the type of device (e.g., emergency lamp, sign, etc.) and its position in the emergency area (e.g., floor, mezzanine, corridor, etc.);
- *Tag classification* indicates the type of the tag (i.e., passive, semi-passive, or active);
- *Accuracy* characterizes the shape of the electromagnetic field set off by the tag antenna;
- *Orientation* is the direction of the tag antenna;
- *Date* represents the last time update of the information stored into the device.

During the mission, the rescuer is tracked by the algorithm running on the processing unit as shown in Fig. 1. The estimates of the rescuers attitude and of the position of the rescuer are performed separately; to this aim, the *Sensory*

System feeds both the *Attitude Filter* and the *Tracking System*. The *Attitude Filter* is based on data retrieved from the inertial platform and it computes the attitude of the rescuer with respect to the Navigation frame. The output of this filter is used by the *Tracking System* to produce the pose (i.e., the position and the heading of the rescuer) also exploiting data collected from both the inertial platform and PILDs. To this end, the *Tracking System* is further decomposed into a prediction-correction Bayesian filter, according to the approach used in robotics localization, where both proprioceptive and exteroceptive sensors are jointly used.

It is worth noticing that all the filters run on-line; however, the loops have different frequencies: the attitude computation depends on the availability of data from the gyroscope, while the inertial prediction is based on the step-event detection, and the RFID refinement is based on the PILD detection event, as explained in the following.

A. The Attitude Filter

The *Attitude Filter* estimates the attitude of the IMU frame (hereafter, the *Body frame*) with respect to the Navigation frame. It is based on an Extended Kalman Filter (EKF) that merges data collected from gyroscopes, accelerometers, and magnetometers. The vector state is represented by means of quaternions: these mathematical entities require less computational effort in recursive updating and avoid the singularity issues that affect angular descriptors, like Euler angles. Quaternions can be defined as $\mathbf{q} = [\eta, \boldsymbol{\epsilon}^T]^T = [\eta, \epsilon_x, \epsilon_y, \epsilon_z]^T$ where η is the scalar part of the quaternion, $\boldsymbol{\epsilon}$ is the vector part of the quaternion.

In the prediction step, the following differential equations are used to evaluate the angular motion of a rigid body:

$$\frac{d}{dt}\mathbf{q} = \boldsymbol{\Omega}\mathbf{q}$$

where $\boldsymbol{\Omega}$ is a skew symmetric matrix

$$\boldsymbol{\Omega} = \frac{1}{2}\begin{bmatrix} 0 & -\omega_z & \omega_y & \omega_x \\ \omega_z & 0 & -\omega_x & \omega_y \\ -\omega_y & \omega_x & 0 & \omega_z \\ -\omega_x & -\omega_y & -\omega_z & 0 \end{bmatrix}^T$$

in which $\boldsymbol{\omega} = [\omega_x, \omega_y, \omega_z]$ represents the angular velocity measured by the IMU in the Body frame and the time-dependence has been omitted for the sake of simplicity.

The corresponding discrete-time model is

$$\begin{cases} \hat{\mathbf{q}}_k = e^{(\boldsymbol{\Omega}_k \Delta t_k)}\hat{\mathbf{q}}_{k-1} = \boldsymbol{\Phi}_k \hat{\mathbf{q}}_{k-1} \\ \hat{\mathbf{q}}_0 = \hat{\mathbf{q}}(0) \end{cases} \tag{1}$$

where $\Delta t_k = [t_{k-1}, t_k]$ is the sampling time interval, $\boldsymbol{\Phi}_k = e^{(\boldsymbol{\Omega}_k \Delta t_k)}$, and $\boldsymbol{\Omega}_k$ is the skew symmetric matrix computed using the vector $\boldsymbol{\omega}_{k-1}$. The quaternion $\hat{\mathbf{q}}_k$ is computed at each sampling time k, starting from the initial condition $\hat{\mathbf{q}}_0$. The initial condition $\hat{\mathbf{q}}_\mathbf{0}$ is computed according to [35] and it is normalized to obtain a unit quaternion. In order to preserve this feature, the estimated value of the quaternion $\hat{\mathbf{q}}_\mathbf{k}$ is further normalized in both the prediction and correction step of the *Attitude Filter*.

It is assumed that, when the rescuer starts the mission, the Body frame corresponds to the Navigation frame (i.e., they are aligned and they share the same origin). Specifically, the $\hat{z}$-axis of the Body frame represents the vertical axis of the rescuer while the $\hat{x}$ and the $\hat{y}$-axes are aligned with the *medio-lateral* and the *antero-posterior* components of the acceleration vector, respectively. At the same time, the z-axis of the Navigation frame is vertical upward and it represents the vertical axis of the environment; the operator moves in the $(x-y)$ plane of the Navigation frame with the x and y-axis aligned with the $\hat{x}$ and the $\hat{y}$-axes of the Body frame at the starting pose (i.e., the rescuer heading is $\theta_0 = 0$). In this configuration, the vector of gravitational acceleration is aligned with the $\hat{z}$-axis and it can be easily compensated. Knowing the attitude of two frames at the starting pose, the attitude of the Body frame can be computed with respect to the Navigation frame by simple rotations.

The covariance matrix of the prediction step can be expressed as:

$$\mathbf{P}^q_{k|k-1} = \boldsymbol{\Phi}_k \mathbf{P}^q_{k-1|k-1}\boldsymbol{\Phi}^T_k + \mathbf{Q}_k \tag{2}$$

where $\mathbf{Q}_k$ is the accuracy of the gyroscopes.

The measurement $\mathbf{z}_k$ is built by stacking the accelerometer and magnetometer measurement vectors as shown in the following equation:

$$\mathbf{z}_k = \left[\mathbf{a}^T_k,\ \mathbf{m}^T_k\right]^T \tag{3}$$

The expected measurement $\hat{\mathbf{z}}_k$ from accelerometers can be computed according to:

$$\hat{\mathbf{a}}_k = h_a(\hat{\mathbf{q}}_{k|k-1}) = \mathbf{K}_a\mathbf{R}(\hat{\mathbf{q}}_{k|k-1})\mathbf{g} \tag{4}$$

where $\hat{\mathbf{a}} = \begin{bmatrix}\hat{a}_x & \hat{a}_y & \hat{a}_z\end{bmatrix}^T$ represents the acceleration in the Body frame, $\mathbf{K}_a$ is the scale factor matrix, $\mathbf{g}$ is the vector of the gravitational acceleration, and $\mathbf{R}(\hat{\mathbf{q}}_{k|k-1})$ is the rotation matrix from the Body frame to the Navigation frame:

$$\mathbf{R}(\hat{\mathbf{q}}_{k|k-1}) = \begin{bmatrix} 2(\eta^2+\epsilon_x^2)-1 & 2(\epsilon_x\epsilon_y - \eta\epsilon_z) & 2(\epsilon_x\epsilon_z - \eta\epsilon_y) \\ 2(\epsilon_x\epsilon_y - \eta\epsilon_z) & 2(\eta^2+\epsilon_y^2)-1 & 2(\epsilon_y\epsilon_z - \eta\epsilon_x) \\ 2(\epsilon_x\epsilon_z - \eta\epsilon_y) & 2(\epsilon_y\epsilon_z - \eta\epsilon_x) & 2(\eta^2+\epsilon_z^2)-1 \end{bmatrix}$$

where the time dependence has been omitted for the sake of clarity. It is worth underlying that data from accelerometers can be used only when the rescuer is still, otherwise the gravitational acceleration cannot be compensated, which is why a validation gate is set up and the acceleration correction is performed only when $\mid ||\mathbf{a}_k|| - ||\mathbf{g}|| \mid < \varepsilon_a$, where $||\cdot||$ is the Euclidean norm, $\mathbf{a}_k$ is the vector of the accelerometer measurements and ε_a is the threshold of the validation gate.

The expected measurement from the magnetometer can be computed according to the following equation:

$$\hat{\mathbf{m}}_k = h_m(\hat{\mathbf{q}}_{k|k-1}) = \mathbf{K}_m\mathbf{R}(\hat{\mathbf{q}}_{k|k-1})\mathbf{d}_m \tag{5}$$

where $\hat{\mathbf{m}} = \begin{bmatrix}\hat{m}_x & \hat{m}_y & \hat{m}_z\end{bmatrix}^T$ represents the magnetic field vector in the Body frame, $\mathbf{K}_m$ is the scale factor matrix and $\mathbf{d}_m$ is the Earth magnetic field represented in the Navigation frame. To prevent the use of magnetometer measures affected by large magnetic disturbances, a matching test is set up, so the

update is performed only when $|\,||\mathbf{m}_k|| - ||\mathbf{d}_m||\,| < \varepsilon_m$ and $||\mathbf{m}_k - \mathbf{m}_{k-1}|| < \varepsilon_{\Delta m}$, where ε_m and $\varepsilon_{\Delta m}$ are the thresholds of the validation gates. When the measurements are reliable, i.e., they have passed the test, the estimate is updated according to the EKF equations. The correspondent covariance matrix is given by:

$$\begin{array}{lcl} \mathbf{S}_k & = & \mathbf{H}_k \mathbf{P}^q_{k|k-1} \mathbf{H}^T_k + \mathbf{V}_k \\ \mathbf{K}_k & = & \mathbf{P}^q_{k|k-1} \mathbf{H}^T_k \mathbf{S}^{-1}_k \\ \hat{\mathbf{q}}_{k|k} & = & \hat{\mathbf{q}}_{k|k-1} + \mathbf{K}_k[\mathbf{z_k} - h(\hat{\mathbf{q}}_{k|k-1})] \\ \mathbf{P}^q_{k|k} & = & (\mathbf{I} - \mathbf{K}_k \mathbf{H}_k)\mathbf{P}^q_{k|k-1} \end{array} \tag{6}$$

where $\mathbf{H}_k$ is the Jacobian of the observation vector $h(\cdot) = [h^T_a(\cdot), h^T_m(\cdot)]^T$, $\mathbf{V}_k$ is the covariance matrix of the measurements, and $\mathbf{K}_k$ is the Kalman gain matrix.

B. The Tracking System

The *Tracking System* recursively provides the position of the rescuer at each sample time j, determined by a step event. It exploits the output of the *Attitude Filter* to compute the heading and the vertical acceleration of the rescuer and it assumes that the initial pose of the rescuer is known. Since the walking activity is the only one considered in this paper, the heading of the rescuer can be easily computed as the rotation with respect to the z-axis of the Navigation frame.

The displacement s_j is computed using the vertical acceleration a^v that can be retrieved by re-projecting the accelerometer signal according to the attitude computed by quaternions. The displacement s_j is determined by using the step detection exploiting the dynamics of the human gait-cycle. For the sake of completeness, the human gait-cycle can be divided in two phases:

- double limb support period;
- single limb support period.

These periods are identified by start and stop events. The first event begins when the first foot strikes and it ends when the other foot's toe-off. The second one starts with the opposite foot toe-off and it ends with the opposite foot strike. The gait cycle, that is the union of the two periods, can be identified by using the local minimum and the local maximum of the vertical acceleration collected by the waist-mounted IMU. After the local minimum and the local maximum identification, the step length is computed by using the following equation [36]:

$$s_j = \beta \sqrt[4]{a^v_{j,M} - a^v_{j,m}} \tag{7}$$

where $a^v_{j,M}$ and $a^v_{j,m}$ are the maximum and the minimum vertical acceleration during a step event j and β is a parameter depending on the user, obtained by using a calibration procedure. Specifically, the parameter β is calibrated by asking the rescuer to walk for a fixed distance. The number of steps performed is used to identify the step length and to set the β parameter accordingly. The step events in calibration and tracking are detected by using a procedure based on zero-crossing and peak detection as in [10], after removing the gravitational acceleration component.

In the prediction step, the position $\hat{\mathbf{p}}_j = [x_j, y_j]^T$ of the rescuer with respect to the Navigation frame and the corresponding accuracy $\mathbf{P}^p_j$ is computed according to the following equation:

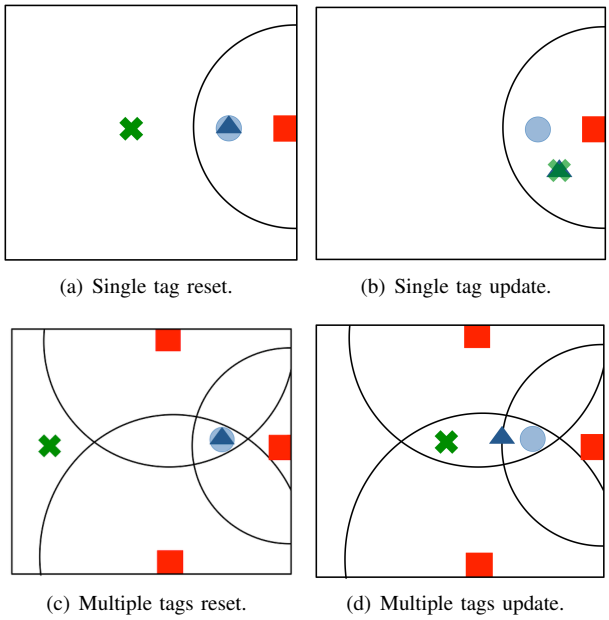

(a) Single tag reset. (b) Single tag update.

(c) Multiple tags reset. (d) Multiple tags update.

Fig. 2. Correction strategies: rescuer position in prediction step (green cross), rescuer position after correction (blue triangle), perceived tags (red squares), radiation lobe center (blue dot), and radiation lobe (black circles).

$$\begin{array}{lcl} \hat{\mathbf{p}}_{j|j-1} & = & \hat{\mathbf{p}}_{j-1|j-1} + \mathbf{l}_j \\ \mathbf{P}^p_{j|j-1} & = & \mathbf{P}^p_{j-1|j-1} + \mathbf{Q}^p_j \end{array} \tag{8}$$

where $\mathbf{l}_j = [s_j cos\bar{\theta}_j, s_j sin\bar{\theta}_j]^T$, $\bar{\theta}_j$ is the average heading during the sampling interval $[j-1, j]$, and $\mathbf{Q}^p_j$ models the inaccuracy of the map in eq. (7). Notice that the duration of each step and therefore the number of samples corresponding to the same sampling interval $[j-1, j]$ is dynamically defined by the step detection procedure. At the end of the inertial prediction phase, the result consists in a rough position estimate affected by sensor drift errors.

The correction step refines the position estimate upon tag detection. According to the REFIRE protocol, the tag provides its own *Geographical Coordinates*, its *Orientation*, and its *Accuracy* w_i. The *Geographical Coordinates* and the *Orientation* are used to compute the center of the radiation lobe $\mathbf{T}^i$ that is exploited to update the position of the rescuer. It is worth noticing that the *Geographical Coordinates* need to be expressed with respect to the Navigation frame: the map can be easily computed if the initial position of the rescuer is georeferenced and if the initial heading with respect to magnetic North is known. According to the model adopted to map the RFID tag measurements, only the position of the rescuer is corrected, since the heading becomes unobservable. Moreover, only context information is used: when a rescuer is in the main radiation lobe of the tag, the reader receives information from the tag and the rescuer's position is updated according to four strategies as shown in Fig. 2. The strategies are designed according to [12], in order to introduce discontinuous measurements in the Bayesian framework.

The first two strategies consider a single tag detection. Specifically, in the first one, shown in Fig. 2(a), the inertial

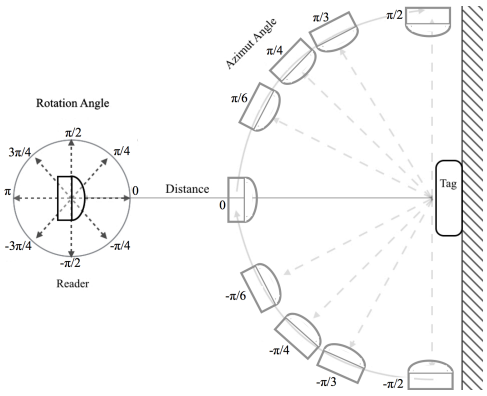

Fig. 3. Parameters for static and dynamic tests.

prediction estimates the rescuers outside the radiation lobe of the perceived tag i. In this case, the position and the accuracy are reset according to the following equations:

$$\begin{array}{rcl} \hat{\mathbf{p}}_{j|j} & = & \mathbf{T}^i \\ \mathbf{P}^p_{j|j} & = & w_i \mathbf{I}_{2\times 2} \end{array} \tag{9}$$

where $\hat{\mathbf{p}}_{j|j}$ represents a new initial position and the covariance $\mathbf{P}_{j|j}$ is set according to the accuracy w_i provided by the tag.

In the second one, shown in Fig. 2(b), the rescuer position is estimated inside the main radiation lobe of the perceived tag i; in this case, the pose is not updated but the accuracy is eventually bounded according to the following equations:

$$\begin{array}{rcl} \hat{\mathbf{p}}_{j|j} & = & \hat{\mathbf{p}}_{j|j-1} \\ \mathbf{P}_{j|j} & = & \left\{ \begin{array}{ll} \mathbf{P}^p_{j|j-1} & \text{tr}[\mathbf{P}^p_{j|j-1}] < w_i^2 \\ w_i \mathbf{I}_{2\times 2} & \text{otherwise} \end{array} \right. \end{array} \tag{10}$$

where $\text{tr}[\mathbf{P}_{j|j-1}]$ represents a measure for the uncertainty.

In the last two cases, the rescuer is inside the main radiation lobe of r tags. If the inertial prediction locates the rescuer outside the radiation lobes, shown in Fig. 2(c), the position $\hat{\mathbf{p}}_{j|j}$ is updated according to the following equations:

$$\begin{array}{rcl} \hat{\mathbf{p}}_{j|j} & = & \bar{\mathbf{T}}^i \\ \mathbf{P}^p_{j|j} & = & \sum_{i=1}^{r} w_i (\mathbf{T}^i - \bar{\mathbf{T}}^j)(\mathbf{T}^i - \bar{\mathbf{T}}^j)^T \end{array} \tag{11}$$

where $\bar{\mathbf{T}}^j$ is the average center of mass of the r tag radiation lobes.

Finally, when the inertial prediction locates the rescuer inside the radiation lobe of a subset of the r perceived tags, the position $\hat{\mathbf{p}}_{j|j}$ is updated according to the following equations:

$$\begin{array}{l} \hat{\mathbf{p}}_{j|j} = \hat{\mathbf{p}}_{j|j-1} + \mathbf{L}_j (\mathbf{T}^j - [\hat{\mathbf{p}}_{j|j-1}]_r) \\ \mathbf{P}^p_{j|j} = \left\{ \begin{array}{ll} \mathbf{P}^p_{j|j-1} & \text{tr}[\mathbf{P}^p_{j|j-1}] < \text{tr}[\mathbf{S}_j] \\ \mathbf{P}^p_{j|j-1} - \mathbf{L}_j \mathbf{S}_j \mathbf{L}_j^T & \text{otherwise} \end{array} \right. \end{array} \tag{12}$$

where $\mathbf{T}^j$ is the block vector of the coordinates retrieved from the r tags, $[\hat{\mathbf{p}}_{j|j-1}]_r$ is a block vector stacking r times the coordinates of the position of the rescuer, $\text{tr}[\mathbf{S}_j]$ is the tags combined uncertainty, and $\mathbf{L}_j$ represents a gain. This gain is computed as: $\mathbf{L}_j = \mathbf{P}_{pz,j} \mathbf{S}_j^{-1}$ where: $\mathbf{P}_{pz,j} = \sum_{i=1}^{r} w_i (\mathbf{T}^i - \hat{\mathbf{p}}_{j|j-1})(\mathbf{T}^i - \bar{\mathbf{T}}^j)^T$ and $\mathbf{S}_j$ is: $\mathbf{S}_j = \sum_{i=1}^{r} w_i (\mathbf{T}^i - \hat{\mathbf{p}}_{j|j-1})(\mathbf{T}^i - \hat{\mathbf{p}}_{j|j-1})^T$ according to the Unscented Kalman Filter equations.

IV. RFID SYSTEM ASSESSMENT

The use of the RFID system for ILP tasks is challenging since it only provides information about the presence of tags in the environment rather than their distance from the reader. RFID systems are commonly used in logistics applications, where high power antennas are used to detect tags equipped with small antennas. In the REFIRE framework, the opposite approach is foreseen, due to design constraints. The reader antenna is positioned on the rescuer: it is small and low power in order to extend the battery life. The tags are embedded in the environment and their size has been increased to host a larger antenna [6].

Assessing the RFID system performances represented a mandatory task in the definition of the proposed hybrid ILP methodology. Therefore, in this Section the results of the RFID assessment are reported. This RFID system is composed of a wearable qID R1240I Bluetooth UHF RFID/BARCODE reader (CAEN RFID), equipped with two directional antennas with horizontal and vertical polarization, and the OMNI-ID Dura 3000 UHF tags (Omni-ID), provided with a large reflective antenna. To better understand the feasibility and the performance of the proposed methodology, a large number of trials have been carried out to outline the behavior of the system under real operating scenarios, since the tags detection performances depend on environmental conditions (i.e., electromagnetic reflections, humidity, temperature, etc). For the sake of space, here are reported only few scenarios, however, a complete assessment for the adopted system has been obtained.

It is worth underlining that RFID tags are used in a range free fashion. In the performed tests, the range between the reader and the tag has been computed by exploiting the RSSI. However, this measure is reliable only if computed by averaging several measures. This requirement is not compliant with the rescue scenario.

The following parameters are used to define a specific operating scenario, as shown in Fig. 3:

- d represents the distance between the tag and the reader. It is set in the range $[0 \sim 350]\, cm$;
- ϑ represents the azimuth between the two devices. When the tag and the reader are faced, $\vartheta = 0$. Here, the following azimuth angles are considered $\vartheta \in \left\{0, \pm\frac{\pi}{6}, \pm\frac{\pi}{4}, \pm\frac{\pi}{3}, \pm\frac{\pi}{2}\right\}\ rad$;
- φ represents the rotation angle of the reader with respect to its vertical axis. The following values are considered $\varphi \in \left\{0, \pm\frac{\pi}{4}, \pm\frac{\pi}{2}, \pm\frac{3\pi}{4}, \pm\pi\right\}\ rad$;
- h_T represents the height of the RFID tag; three different heights are considered, so $h_T \in \{149, 187, 220\}\ cm$, according to the heights of the emergency signs;
- h_R represents the height of the RFID reader; several values are considered according to the user heights;
- e represents the emission power of the reader. It can be set via the reader software with respect to the maximum power $12.5\, mW$ to high power (100%), medium power (66%) and low power (33%).

The tests performed can be divided into two classes: *static* and *dynamic* tests. In these tests, different indexes are used to

TABLE I
RFID EFFICIENCY η_{eff} [%] VS DISTANCE d $[cm]$ USING DIFFERENT POWER LEVEL e (LOW, MEDIUM, HIGH) AT $h_T = 149$.

	50	**100**	**150**	**200**	**250**	**300**	**350**	**400**
Low	100	100	50	20	0	0	0	
Medium	100	100	100	100	75	0	0	0
High	100	100	100	100	100	50	25	0

TABLE II
RFID EFFICIENCY η_{eff} [%] VS DISTANCE d $[cm]$ USING DIFFERENT POWER LEVEL e (LOW, MEDIUM, HIGH) AT $h_T = 220$.

	50	**100**	**150**	**200**	**250**	**300**	**350**	**400**
Low	50	75	10	0	0	0	0	0
Medium	50	100	30	5	0	0	0	0
High	50	90	40	50	0	0	0	0

evaluate the efficiency of the system, as detailed below.

A. Static Tests

The static tests aim at setting the performance of the system into indoor environments, considering a stationary reader. The main outcome of these tests is the definition of the radiation lobe of a tag in real operating conditions: tests, indeed, were performed in office like environments, where reflections warp the nominal radiation lobe.

During the trials, the reader is fixed on a mobile platform and located in different positions near a tag: tests performed in similar operating conditions have been averaged. In all the trials, an average height is considered, so $h_R = 140\,cm$.

The efficiency η_{eff} is defined as the percentage of the echoes over the queries sent:

$$\eta_{eff} = \frac{n_e}{n_q} \cdot 100 \tag{13}$$

where n_e is the number of echoes detected and n_q the total number of queries.

The first set of trials aims at evaluating the performance of the system, using different power levels. They are obtained by locating the reader in front of the tag (i.e., $\vartheta = 0\,rad$ and $\varphi = 0\,rad$) and by moving forward and backward the mobile platform, changing the parameter d. For the tag, two different heights (i.e., $h_T \in \{149, 220\}\,cm$) have been considered. The outcome of the trials is reported in Tab. I and II: by considering both high and medium level, the same efficiency is obtained, while the performance is downgraded by using the low level. To limit the energy consumption, the power level needs to be set to medium power. It is worth also noticing that the higher the difference $|h_T - h_R|$, the lower the efficiency.

The second set of trials aims at defining the efficiency of the RFID system, considering different rotation angle φ. In Tab. III, the results considering $e = 66\%$, $h_T = 149\,cm$, $\vartheta = 0\,rad$ are presented.

Looking at Tab. III, the first column ($\varphi = 0\ rad$) reports the same results of the test in Tab. I and the devices are perfectly faced; the efficiency quickly decreases in the same way when the reader is rotated clockwise or counter-clockwise. Some outliers are obtained when the reader is completely rotated ($\varphi = \frac{3\pi}{4}\ rad$ and $\varphi = \pi\,rad$) due to reflections.

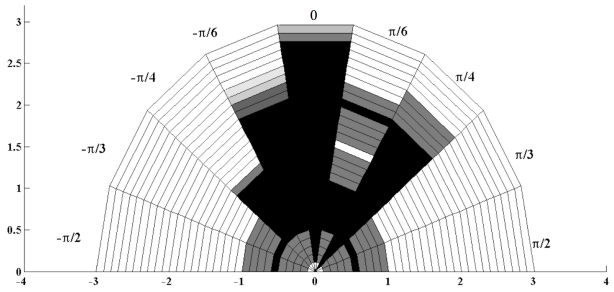

Fig. 4. Percentage of successful readings. Black represents the $70 - 100\%$ and white is $0 - 30\%$.

TABLE III
RFID EFFICIENCY η_{eff} [%]: DISTANCE d $[cm]$ VS ROTATION ANGLE φ $[rad]$

	0	$\frac{\pi}{4}$	$\frac{\pi}{2}$	$\frac{3\pi}{4}$	π	$-\frac{3\pi}{4}$	$-\pi$	$-\frac{\pi}{4}$
50	100	100	0	100	75	0	0	100
100	100	100	0	100	30	0	0	100
150	100	75	0	50	50	0	0	20
200	100	0	0	30	0	0	0	0
250	80	0	0	0	0	0	0	0
300	0	0	0	0	0	0	0	0

Finally, several tests have been carried out to characterize the efficiency behavior when the value of the azimuth angle ϑ changes. In this trial, the reader height is set to $h_R = 160\,cm$, the tag height to $h_T = 220\,cm$,, the power to $e = 66\%$, and the reader point slightly upward. A result of these tests is reported in Fig. 4: the tag has a fixed location (i.e., the origin of the reference frame) and orientation, while the reader moves in the surroundings, changing the distance $d \in [0 \sim 350]\,cm$.

The performed tests point out that in static conditions, the maximum range of the radiation lobe of the RFID system can be assumed to $r = 250\,cm$ with a maximum angle of $\alpha = \pm\frac{\pi}{3}\,rad$: the direction of the lobe strongly depends on the orientation of the tag.

TABLE IV
TAG DETECTIONS IN DOOR CROSSING TESTS

(a) e = 66% v_u = 1 m/s

Path	**0 – 1 m**	**1 – 2 m**	**2 – 3 m**	**TOT**
AB	0	0	1	1
CD	0	1	2	3
EF	0	1	2	3
BA	0	0	1	1
DC	0	0	2	2
FE	0	0	0	0

(b) e = 66% v_u = 2 m/s

Path	**0 – 1 m**	**1 – 2 m**	**2 – 3 m**	**TOT**
AB	0	0	1	1
CD	0	0	2	2
EF	0	0	1	1
BA	0	0	0	0
DC	0	0	0	0
FE	0	0	0	0

TABLE V
TAG DETECTIONS IN THE CORRIDOR TEST

Path S–M			Path M–E		
TAG 1	**TAG 2**	**TAG 3**	**TAG 3**	**TAG 2**	**TAG 1**
2	9	0	3	9	0

TABLE VI
TAG DETECTIONS IN THE OPEN SPACE TEST

TAG 1	TAG 2	TAG 3
11	0	5

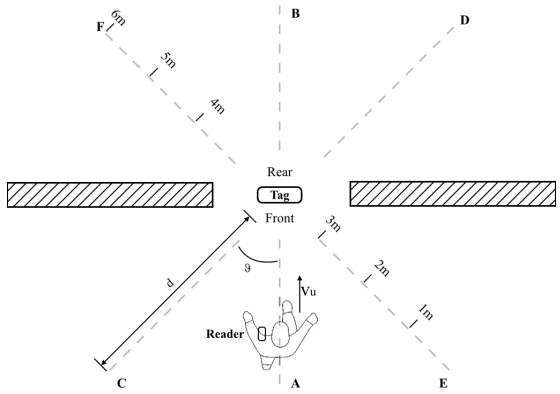

Fig. 5. Door crossing tests.

B. Dynamic Tests

The aim of the dynamic tests is to evaluate the performance of the RFID system during the user's motion. To this end, different scenarios are considered: in the first set of trials, door crossing test is considered, in the second, and third trials the user walking in a office-like environment is addressed. In all trials, the power is set to $e = 66\%$, while the remaining parameters change due to the walking dynamics; the user speed v_u is considered.

In these tests, the efficiency η_{eff} is measured as $\eta_{eff} = n_e$ since the reader is not always in a radiation lobe of a tag during the motion, so there is no need to consider the total number of queries.

In the first trial, the reader is placed on the left shoulder of a user walking across a door along three different paths, as shown in Fig. 5. The results of these tests are averaged and approximated to the lower integer over 10 path executions. They are reported in Tab. IV: the number of detections during the forward walking are collected, considering two different speed, $v_u = 1\,m/s$ and $v_u = 2\,m/s$. As it can be noticed from the results, a larger number of detections is retrieved walking at a lower speed, since, under this operating condition, the reader is in the tag radiation lobe for a longer time, however some detections are available also at a higher speed. It is worth noticing that, during the trial, the user passes across a fire door (which is a metal door). Due to the large interference, the reader is able to retrieve information only when the user is far from the door.

In the second trials, the user walks along a corridor as shown in Fig. 6(a): the overall length of the path is $l = 34\,m$, the user speed is about to $v_u = 1\,m/s$. The reader is placed on the left shoulder of the user, considering $h_R = 140\,cm$. The three tags used in the experiment are located on the columns, their height is $h_T = 220\,cm$ and their orientation with respect to the vertical z-axis of the Navigation frame are respectively $\varphi_T = \frac{\pi}{16}\,rad$, $\varphi_T = \frac{\pi}{12}\,rad$, and $\varphi_T = \frac{\pi}{6}\,rad$ for the first, second and third tag.

The detections of the reader during the test are reported, in Tab. V. It is worth noticing that the detections number of the second tag is greater than the others, due to the presence of a metal door reflecting the electromagnetic signal.

In the third dynamic test a walk in an open space is performed as shown in Fig 6(b). The user walks along a $26\,m$ long path at a constant speed $v_u = 1\,m/s$, and wears the RFID reader on the left shoulder. Three tags are considered: they have the same orientation with respect to the z-axis of the Navigation frame $\varphi_T = 0\,rad$, however the three tags are located at different heights, which are respectively $h_T = 149\,cm$, $h_T = 187\,cm$, and $h_T = 220\,cm$ for the first, second and third tag.

The number of echoes retrieved from each tag during the experiment is reported in Tab. VI. The second tag is not detected since the radiation lobe of the RFID reader does not intersect the radiation lobe of the tag itself.

As proved by the assessment, the RFID technology represents a good candidate for hybrid localization. In both static and dynamic conditions, the information retrieved from the RFID system is crucial to correct the position estimate supplied by the inertial system, and to reduce the position error. Specifically, according to the static and dynamic tests, the configuration parameters (i.e., $e = 66\%$, $h_R = 140\ cm$, $h_T = 220\ cm$) and the radius of the radiation lobe (i.e., $d_{max} = 250\ cm$) are retrieved. The dynamic tests confirmed the outcomes of the static assessment: assuming the same configuration and a user walking at normal speed, the reader is able to perceive the tag up to $d_{max} = 250\ cm$. Since the position error provided by the inertial navigation grows unbounded and it can reach several tens of meters in long lasting missions, the hybrid approach provides a more reliable result by reducing the maximum position error to $\pm 250\ cm$ and by exploiting a sufficiently dense network of RFID tags.

V. EXPERIMENTAL RESULTS

Several experimental tests have been carried out to prove the effectiveness of the HIPS into different indoor scenarios. For the sake of space, this paper only considers an office like scenario. The testing environment is composed of a long ring-shaped corridor bounds by rooms. This environment has been selected for its closed-loop layout, that allows a better assessment of the performance of the localization algorithm. According to the EU Directive 92/58/EEC, which defines the shape, the color, and the location of the safety signs, the environment is equipped with 30 emergency signs, however, as shown in Fig. 7 only 9 tags having $h_T = 220\ cm$ have been deployed. As illustrated in section III-A, the Navigation frame is fixed in the testing smart environment: its origin corresponds to the first check point in Fig. 7, the z-axis is vertical upward,

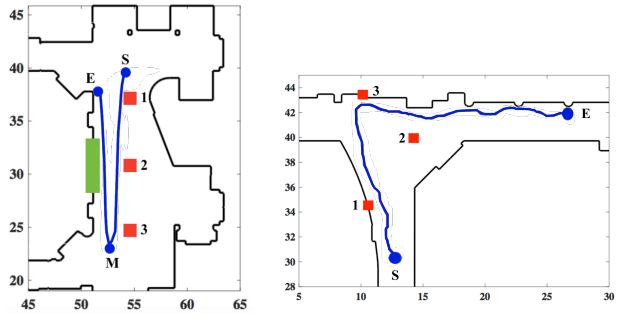

(a) Corridor test: user path (blue solid line), tags (red squares) and metal door (green square).

(b) Open space test: user path (blue solid line) and tags (red squares).

Fig. 6. Dynamic tests: S is the starting point, E is the ending point, unit on $(x-y)$-axes is $[m]$.

TABLE VII
PARAMETERS INITIALIZATION.

PARAMETER	INITIALIZATION VALUE
ε_a	$0.1\ m/s^2$
ε_m	$10\ \mu T$
$\varepsilon_{\Delta m}$	0.4
$\mathbf{V}_0$	$diag\{0.01, 0.11, 0.02, 0.19, 0.18, 0.12\}$
$\mathbf{Q}_0^p$	$diag\{0.03, 0.03\}$

the x and the y-axes are parallel to the starting poses of the Body frame.

Furthermore, 6 check points in known locations are used to evaluate the performance of the system. The accuracy of HIPS is measured as $||\hat{\mathbf{p}}_{j|j} - \mathbf{p}_i||$, i.e., the Euclidean distance between the estimated user position and the position of the i-th check point $\mathbf{p}_i$, where $i \in \{A, \cdots, F\}$. This key performance indicator is largely used in indoor localization competitions.

During experimental trials, the rescuer is equipped with a waist-worn iNEMO STEVAL-MKI062V2 device (STMicroelectronics) and the RFID qID R1240I reader, while the Omni-ID tags are deployed in the environment. Both the IMU and the reader are connected to the same laptop by means of high speed USB and Bluetooth, respectively. The sampling frequency of the iNEMO is 100 *Hz*, the one of RFID reader is 10 *Hz*, and a step is detected at $\sim$2 *Hz*. To this end, a synchronization procedure has been performed for data alignment. In these trials, the RFID system detection area is computed according to the results shown in Fig. 4, so the main radiation lobe is supposed to have a range of $d_{max} = 250$ *cm*. A MATLAB toolbox has been developed by the authors for data pre-processing and for the HIPS algorithm implementation. In Tab. VII, the parameters used to initialize the HIPS are collected during the experiments.

The vector $\mathbf{d}_m$ is the local Earth magnetic field: it is set by averaging data from magnetometer at the beginning of the mission, when the rescuer is supposed to stay still for 60 s at his starting pose. The parameters ε_a and ε_m are determined by selecting the maximum variance of the acceleration and the magnetic field vector measured by the IMU with respect to $\mathbf{g}$ and $\mathbf{d}_m$, respectively. At the same time, we selected $\varepsilon_{\Delta m}$ by computing the maximum variation between two consecutive values of the magnetic field vector measured by the IMU, when the operator moves in the testing environment. The same procedure has been used to define the initial values $(\mathbf{V}_0, \mathbf{Q}_0^p)$ of the covariance matrix of the measurements $\mathbf{V}_j$, and of the model uncertainty $\mathbf{Q}_j^p$.

The scale factor matrices for the accelerometer and magnetometer are $\mathbf{K}_a = diag\{k_a^x, k_a^y, k_a^z\} = diag\{1.0478, 0.9990, 1.0068\}$, $\mathbf{K}_m = diag\{k_m^x, k_m^y, k_m^z\} = diag\{1.0082, 0.9987, 1.0567\}$, respectively. Both matrices are the results obtained when the iNEMO sensor was calibrated using the procedure in [33]. The scale factor matrix $\mathbf{K}_m$ for the magnetometer has been determined by using the well-known method proposed in [2].

The trial shown in Fig. 7 represents a penetrating mission along the corridor. During the experiment, the user explores the environment like a rescuer, by executing about 500 m.

The objective of this trial is to analyze the improvement provided by the RFID technology together with the inertial one, to this end different deployment configurations of the RFID tags are considered. The results of the PDR are presented in Fig. 7(a): it can be noticed that the PDR is not suitable to achieve room level accuracy, since the tracking error grows along the path. On the other hand, by using all the tags installed in the environment (i.e., 9 tags) the accuracy improves and the tracking system fits the rescuer requirements, as shown in Fig. 7(b). It is worth noticing, that *Rule d* is activated on tags 7 and 8, since the radiation lobe are overlapped, *Rule a* or *Rule b* are activated on the remaining tags, while *Rule c* is not considered due to the path executed by the rescuer. In Fig. 7(c), the impact of a reduced set of tags (i.e., 6 tags located on the corner, $\{1, 2, 4, 5, 6, 9\}$) is shown: the results are downgraded with respect to the estimate computed by using 9 tags, however, the accuracy still fulfils the requirements. To better highlight the importance of the deployment of the tags, the path retrieved by using 5 tags (i.e., $\{1, 3, 5, 7, 8\}$) is reported in Fig. 7(d): only the tags on the corridor are considered active and the estimate is not able to locate the rescuer with a room-level localization accuracy. It worth underlining that the number of tags considered to retrieve the results in Fig. 7(b) is a reduced set of the number of tags. This shows that the proposed system is effective even if only a small fraction of the foreseen tags is available. Moreover, the use of tags also mitigates the effect of heading drift on position error, as shown in Fig. 7.

In Tab. VIII, the estimate errors on the check point are reported. Considering only PDR, the error accumulated is 16 m. When all the tags are used to refine the position, the maximum error is reduced up to 2.6 m. However, it is worth noticing that the accuracy of the estimation depends on both the number and the location of active tags. When the tags are placed on the corner, as shown in Fig. 7(c), the maximum estimate error is ~ 4 m. The same performance index largely increases (~ 13 m) by deploying the tags along the corridor.

The impact of the RFID correction on the estimate applying *Rule a* and *Rule b* is highlighted in Fig. 8, where the HIPS output along the x-axis of the Navigation frame is depicted. It can be noticed that some discontinuities arise in the estimated path. Specifically, the correction step inside the A area does

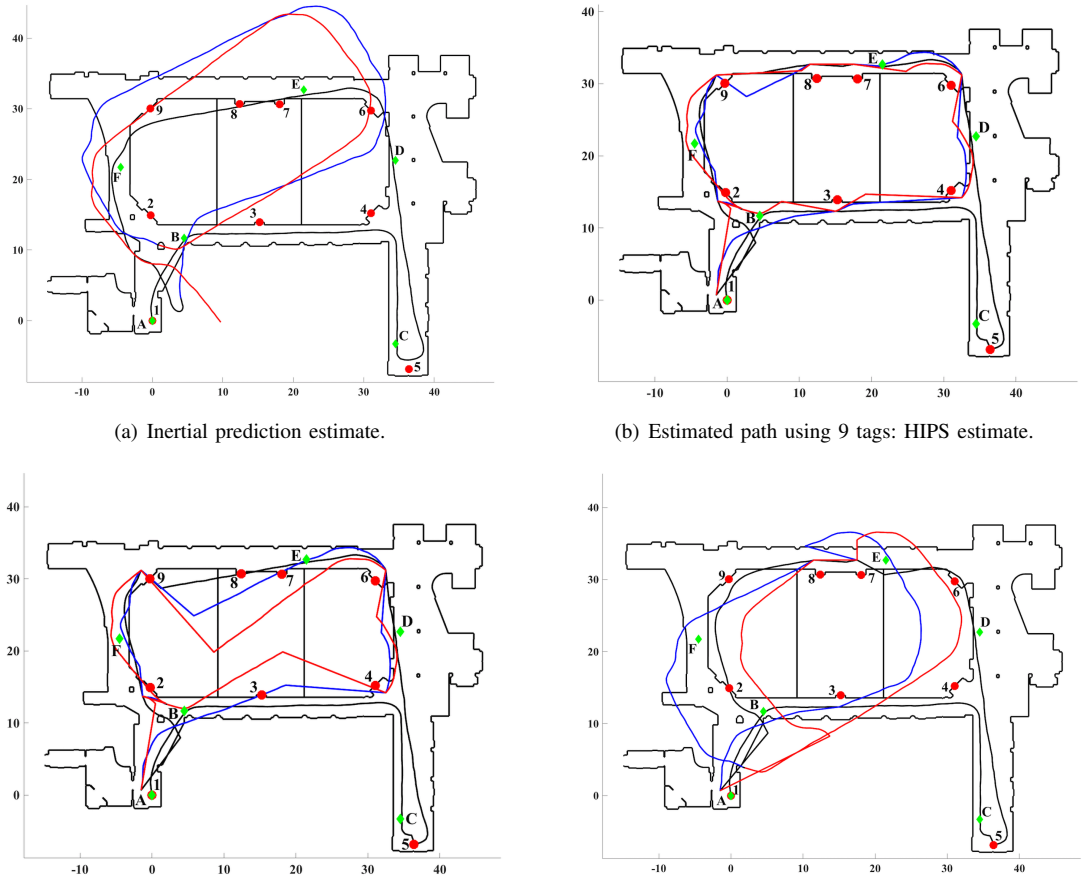

(a) Inertial prediction estimate.

(b) Estimated path using 9 tags: HIPS estimate.

(c) Estimated path using 6 tags: HIPS estimate.

(d) Estimated path using 5 tags: HIPS estimate.

Fig. 7. Indoor results in office like environment: HIPS estimate (black line for the first round, blue line for the second one, and red line third one), check points position (green stars), and tags position (red dots).

TABLE VIII
PREDICTION AND CORRECTION EUCLIDEAN ERRORS $[m]$

	B	C	D	E	F	A	B	D	E	F	B	D	E	F	A
PREDICTION	0.56	0.29	0.72	1.79	7.01	4.42	3.52	15.89	11.50	6.01	1.42	16.13	11.60	9.25	9.71
CORRECTION ALL TAGS	0.56	0.28	0.72	0.38	1.96	1.65	2.11	2.62	0.18	2.4	0.41	2.06	1.60	1.34	1.65
CORRECTION CORNER TAGS	0.56	0.28	0.72	0.47	2.82	1.65	2.53	2.62	0.18	3.58	0.95	1.72	3.35	4.28	1.65
CORRECTION CORRIDOR TAGS	0.56	0.28	0.72	2.05	4.8	1.65	3.30	13.34	11.12	11.19	7.84	10.7	4.54	9.43	1.65

not change the estimate along the $x-$axis, since the output of the prediction step is accurate and *Rule b* is applied. On the contrary, a discontinuity can be appreciated in the correction inside the B area, when *Rule a* is applied.

During the experiment, the conditions to correct the heading using magnetometer are met on the 40% of the measurements. It is worth noticing that in the trials the source of errors depends on the heading error, while the error on the length of the path is less than 4 m by using PDR. Since the heading is not corrected by tags, a residual bias affects the estimate downgrading the overall results.

VI. CONCLUSION

This paper presents the design and implementation of a hybrid localization system for first responder for deep indoor applications. The HIPS methodology relies on the well-known localization scheme adopted in robotics: both proprioceptive and exteroceptive sensors are exploited. The first one, represented by a 6-DoF IMU, is used to provide a rough position estimate of the operator, while the second one, represented by RIFD tags and the reader, is used to refine the prediction estimate. This approach allows to suitably reduce the drift error in the pose estimate by achieving a room level accuracy.

Designing the system, a great importance has been given to the calibration of each sensors. The RFID system has been calibrated by testing reader and tags under several operating conditions. Results from the calibration procedure allows to improve the overall accuracy of the localization filter, suitable to locate first responders during mission.

Future works will be devoted to further improve the accuracy by using a pre-deployed network composed of active tags and deeply investigate the convergence of the Bayesian filters using context-aware information. Moreover, the heading correction will be included to obtain more robust results.

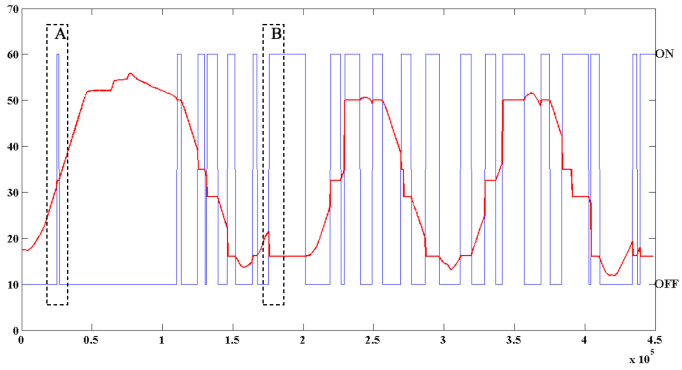

Fig. 8. Position estimate along x-axis $[m]$ (red line) and tag activation pattern (blue, $ON = 60$ – $OFF = 10$) vs time $[ms]$

REFERENCES

[1] S. Aman, C. D. Quint, A. Abdelgawad, and K. Yelamarthi, "Sensing and classifying indoor environments: An IoT based portable tour guide system," *IEEE Sensors Applications Symposium (SAS)*, Glassboro, pp. 1-6, 2017.

[2] M. J. Caruso, "Applications of magneto-resistive sensors in navigation systems", *SAE Technical Paper*, no. 970602, 1997.

[3] K. Deepika, J. Usha, "Design & development of location identification using RFID with Wi-Fi positioning systems," *9th Int. Conf. on Ubiquitous and Future Networks (ICUFN)*, Milan, pp. 488-493, 2017.

[4] Z. Deng, Y. Yu, X. Yuan, N. Wan, L. Yang, "Situation and development tendency of indoor positioning", *China Communications*, vol. 10, no. 3, pp. 42–55, 2013.

[5] R. Faragher, R. Harle, "An Analysis of the Accuracy of Bluetooth Low Energy for Indoor Positioning Applications," *Proc. of the 27th Int. Technical Meeting of The Satellite Division of the Institute of Navigation (ION GNSS+ 2014)*, Tampa, Florida, pp. 201-210, 2014.

[6] L. Faramondi, F. Inderst, F. Pascucci, R. Setola, and U. Delprato, "An Enhanced Indoor Positioning System for First Responders", *IEEE International Conference on Indoor Positioning and Indoor Navigation (IPIN)*, pp. 1-8, 2013.

[7] L. Filardo, F. Inderst, F. Pascucci, "C-IPS: a Smartphone based Indoor Positioning System", *IEEE International Conference on Indoor Positioning and Indoor Navigation (IPIN)*, 2016.

[8] A. Ganz, J. Schafer, S. Gandhi, E. Puleo, C. Wilson, and M. Robertson, "PERCEPT Indoor Navigation System for the Blind and Visually Impaired: Architecture and Experimentation," *International Journal of Telemedicine and Applications*, vol. 19, 2012.

[9] M. Hasani, J. Talvitie, L. Sydanheimo, E. S. Lohanm, and L. Ukkonen, "Hybrid WLAN-RFID Indoor Localization Solution Utilizing Textile Tag," *IEEE Antennas and Wireless Propagation Letters*, vol. 14, pp. 1358-1361, 2015.

[10] R. Harle, "A survey of indoor inertial positioning systems for pedestrians," *IEEE Communications Surveys & Tutorials*, vol. 15, no. 3, pp. 1281–1293, 2013.

[11] D. Hauschildt, N. Kirchhof, "Advances in thermal infrared localization: Challenges and solutions", *IEEE International Conference on Indoor Positioning and Indoor Navigation (IPIN)*, pp. 1-8, 2010.

[12] R. Ivanov, N. Atanasov, M. Pajic, G. Pappas and I. Lee, "Robust estimation using context-aware filtering", *53rd Annual Conference on Communication, Control, and Computing (Allerton)*, pp. 590-597, 2015.

[13] C. Jihong, "Patient positioning system in hospital based on Zigbee", *Intelligent Computation and Bio-Medical Instrumentation (ICBMI)*, pp. 159–162, 2008.

[14] N. Y. Keong, K. S. Chieh, M. F. Burhan, N. Balasubramaniam and N. M. Din, "RFID and ZigBee integrated environment for indoor localization," *Proc. of 4th Int. Conf. on Engineering Technology and Technopreneuship (ICE2T)*, Kuala Lumpur, pp. 213-217, 2014.

[15] A. Li, Y. Li, "Portable RFID Location System in Security Field," *Intern. Conf. on Cyber-Enabled Distributed Computing and Knowledge Discovery (CyberC)*, Chengdu, pp. 413-417, 2016.

[16] N. Li, B. Becerik-Gerber, B. Krishnamachari, L. A. Soibelman, "BIM centered indoor localization algorithm to support building fire emergency response operations", *Automation in Construction*, vol. 42, pp. 78–89, 2014.

[17] D. Lieckfeldt, J. You, and D. Timmermann, "Exploiting RF-Scatter: Human Localization with Bistatic Passive UHF RFID-Systems," *Proc. of IEEE Int. Conf. on Wireless and Mobile Computing, Networking and Communications*, Marrakech, pp. 179-184, 2009'.

[18] C. J. Lin, T. L. Lee, S. L Syu, B. W Chen, "Application of intelligent agent and RFID technology for indoor position: Safety of kindergarten as example", *Machine Learning and Cybernetics (ICMLC)*, vol. 5, pp. 2571–2576), 2010.

[19] Y. Liu, Y. Zhao, L. Chen, J. Pei, J. Han, "Mining frequent trajectory patterns for activity monitoring using radio frequency tag arrays", *IEEE Transactions on Parallel and Distributed Systems*, vol. 23, no. 11, pp. 2138–2149, 2012.

[20] L. Miller, "Indoor navigation for first responders: a feasibility study", *National Institute of Standards and Technology, Wireless Communication Technologies Group*, 2006.

[21] R. Minutolo, L. A. Annoni, "Indoor localization with multi sensor data fusion in Ad Hoc mobile scenarios", *IEEE International Conference on Ultra-WideBand (ICUWB)*, pp. 403–408, 2014.

[22] L. M. Ni, D. Zhang, M. R. Souryal, "RFID-based localization and tracking technologies," *IEEE Wireless Communications*, vol. 18, no. 2, pp. 45–51, 2011.

[23] NIOSH, "Fatality Assessment and Control Evaluation Investigation Report # F2006-19". Accessed: June, 2017. [Online]. Available: http://www.cdc.gov/niosh/fire/pdfs/face200619.pdf.

[24] NIOSH, "Fatality Assessment and Control Evaluation Investigation Report # F2007-18'. Accessed: June, 2017. [Online]. Available: http://www.cdc.gov/niosh/fire/pdfs/face200718.pdf.

[25] L. Ni, Y. Liu, Y. Lau, A. Patil, "LANDMARC: indoor location sensing using active RFID", *Wireless Networks*, vol. 10, no. 6, pp. 701–710, 2004.

[26] N. Pathanawongthum, P. Cherntanomwong, "Empirical evaluation of RFID-based indoor localization with human body effect," *Proc. of 15th Asia-Pacific Conference on Communications*, Shanghai, pp. 479-482, 2009.

[27] W. Ruan, Q. Z. Sheng, L. Yao, T. Gu, M. Ruta, and L. Shangguan, "Device-free indoor localization and tracking through Human-Object Interactions," *Proc. of IEEE 17th Int. Sym. on World of Wireless, Mobile and Multimedia Networks (WoWMoM)*, Coimbra, pp. 1-9, 2016.

[28] J. Ruppelt, P. Merz, G. F. Trommer, "IndoorGuide – A multi sensor pedestrian navigation system for precise and robust indoor localization", *Inertial Sensors and Systems (ISS)*, pp. 1–20, 2016.

[29] M. Saad, C. Bleakley, T. Ballal, S. Dobson,"High-accuracy reference-free ultrasonic location estimation", *IEEE Transactions on Instrumentation and Measurement*, vol. 61, pp. 1561–1570, 2012.

[30] C. Sánchez, S. Ceriani, P. Taddei, E. Wolfart, V. Sequeira, "STeAM sensor tracking and mapping", *Second Annual Microsoft Indoor Localization Competition*, 2015.

[31] T. Sanpechuda, L. Kovavisaruch, "A review of RFID localization: Applications and techniques", *IEEE International Conference on Electrical Engineering/Electronics, Computer, Telecommunications and Information Technology (ECTI-CON)*, vol. 2, pp. 769–772, 2008.

[32] P. Santos, S. Crisóstomo, T. Abrudan, J. Barros, "On-the-fly deployment of wireless sensor networks for indoor assisted guidance", *Proc. of Inter. Conf. on Cyber-Physical Systems, Networks, and Applications (CPSNA)*, pp. 1–4, August, 2013.

[33] D. Tedaldi, A. Pretto, E. Menegatti, "A robust and easy to implement method for IMU calibration without external equipments", *IEEE International Conference on Robotics and Automation (ICRA)*, pp. 3042–3049, 2014.

[34] E. Trucco, K. Plakas, "Video tracking: a concise survey", *IEEE Journal of Oceanic Engineering*, vol. 31, pp. 520–529, 2006.

[35] R. G. Valenti, I. Dryanovski, Jizhong Xiao, "Keeping a Good Attitude: A Quaternion-Based Orientation Filter for IMUs and MARGs", *Sensors*, pp. 19303–19330, 2015.

[36] H. Weinberg, "Using the ADXL202 in pedometer and personal navigation applications," *Analogue Devices AN-602 application note*, vol. 2, no. 2, pp. 1–6, 2002.

[37] Q. Yang, S. J. Pan, V. W. Zheng, "Estimating Location Using Wi-Fi", *IEEE Intelligent Systems*, vol 23, pp. 8–13, 2008.

[38] Z. Xiao, Y. C. Wang, B. Tian, Q. Yu, C. K. Yi, "Development and prospect of ultra-wideband localization research and application", *Dianzi Xuebao (Acta Electronica Sinica)*, vol. 39, no. 1, pp. 133-141, 2011.

[39] S. Zhou, J. K. Pollard, "Position measurement using Bluetooth", *IEEE Transactions on Consumer Electronics*. vol. 52, pp. 555-558, 2006.

Francesca De Cillis received the BE in Biomedical Engineering (2005), the PhD in Engineering (2016) from the University Campus Bio-Medico of Rome, and the MS in Biomedical Engineering (2009) from the University of Rome "La Sapienza". She attended a two year post graduate course in Robotics and Intelligent Systems (2011) at the University of Naples "Federico II", and a one year post graduate course in Homeland Security (2017) at the University Campus Bio-Medico of Rome. She gained several years of experience in both academia and industry, working in National and International research projects devoted to different application domains (critical infrastructure protection, situation awareness, indoor localization). She is currently working as security system engineer in an international telecommunication company.

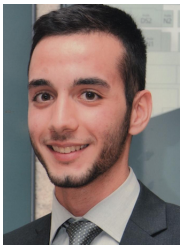

Luca Faramondi received the MS in Management and Automation Engineering (2013) and the PhD in Computer Science and Automation Engineering (2017) from the University of Roma Tre. He is currently Post-Doc Fellow at Complex Systems and Security (COSERITY) Lab at the University Campus Bio-Medico of Rome. He is involved in several National and European projects about the critical infrastructure and indoor localization. His research interests include the identification of network vulnerabilities, the cyber physical systems, and the optimization problems.

Federica Inderst received the MS in Management and Automation Engineering (2013) and the PhD in Computer Science and Automation Engineering (2017) from the University of Roma Tre. She was visiting student at the Georgia Institute of Technology (2016) in Atlanta and IFSTTAR (2016) in Nantes. She is currently with the Department of Engineering of the University of Roma Tre as adjoint researcher. She is involved in several projects about the indoor localization and autonomous train navigation. Her research interests are in field of the indoor localization and navigation system, the wireless sensor network, and the human-robot interaction.

Stefano Marsella received the MS in Civil Engineering (1986) from the University of Rome "La Sapienza". In 1988 has joined the National Fire Service (CNVVF) as Officer. He has been involved in rescue activities and fire protection controls until 1991. From 1991 to 2003 has been working in the fire safety regulations. In 2003 has been appointed Manager of fire services (Arezzo Province). From 2005 to 2011 has been head of the IT services of the CNVVF. From 2011 to 2014 has been responsible for the fire services of the Perugia Provinces. Is currently Director of the National Fire Academy. From 2007 is involved in EU funded research projects. From 2014 coordinates the CNVVF participation to EU funded research projects. Has published several books and papers concerning fire protection and the use of IT to the preparedness and management of emergencies concerning cultural heritage and mass evacuation.

Marcello Marzoli received the MS in Aerospace Engineering from the University of Rome "La Sapienza", since 1990 he works for the Italian Ministry of Interior, Department of Fire Corps and he is currently Fire Captain. He served at the National Control Centre, the Air Service, the IT office and the National Fire Academy. Since 2001, he participates to several European and National R&D projects focused on satellites, indoor location, control centers? interoperability, mass evacuation and cultural heritage protection. He acted as EU expert evaluator for R&D projects and as member of the NFPA 1616 Committee on Mass Evacuation and Sheltering. Inventor and assignee of Italian patents, he has published several papers.

Federica Pascucci received the MS in Computer Science and Automation Engineering (2000) from the University of Roma Tre and the PhD in System Engineering (2004) from the University of Rome "La Sapienza". Since 2005, she is with the Department of Engineering of the University of Roma Tre as Assistant Professor. She was visiting scholar at the University of Örebro (2003) and at the University of Cyprus (2013). She is the principal investigator in several EU funded projects. Her research interests include wireless sensor networks, indoor localization, cyber physical systems, industrial control systems, and critical infrastructure protection. She has published more than 80 journal and conference papers, receiving three best conference paper awards.

Roberto Setola received the MS in Electronic Engineering 1992) and the PhD in Control Engineering (1996) from the University of Naples "Federico II". From 1999 to 2004, he served at the Italian Prime Minister's Office. He is currently Associate Professor of Automatic Control at the University Campus Bio-Medico of Rome, where he is the head of the Complex System and Security (COSERITY) Laboratory and the Director of the Postgraduate Master Program in Homeland Security. He has been the coordinator of four EU projects and he authored nine books and more than 200 scientific papers. His main research interests are the modeling and control of complex systems and critical infrastructure protection.